Applied Ocean Research 95 (2020) 102019

Contents lists available at ScienceDirect

Applied Ocean Research

journal homepage: www.elsevier.com/locate/apor

FIM - flow-induced motions of four-column platforms

Rodolfo T. Gonçalves[a,*], Nicole H. Hannes[b], Maria E.F. Chame[c], Pedro P.S.P. Lopes[c], Shinichiro Hirabayashi[d], Hideyuki Suzuki[a]

[a] OSPL – Ocean Space Planning Laboratory, Department of Systems Innovation, School of Engineering – The University of Tokyo, 7-3-1 Hongo, Bunkyo-Ku, Tokyo 113-8656, Japan
[b] Department of Mobility Engineering, Federal University of Santa Catarina, Joinville, SC, Brazil
[c] TPN – Numerical Offshore Tank Laboratory, Department of Naval Architecture and Ocean Engineering, Escola Politécnica - University of São Paulo, São Paulo, SP, Brazil
[d] OSPL – Ocean Space Planning Laboratory, Department of Ocean Technology, Policy, and Environment, School of Frontier Sciences – The University of Tokyo, Kashiwa-Shi, Chiba, Japan

ARTICLE INFO

Keywords:
Flow-induced motions
Vortex-induced motions
Galloping
Four-column platforms
Spacing ratio
Model tests
Circular column
Square column
Diamond column

ABSTRACT

Experiments regarding the FIM – flow-induced motion on an array of four floating cylinders with low aspect ratio, $H/L = 1.5$, and three different distances between column centers, or spacing ratio, S/L=2, 3 and 4, were carried out in a towing tank; where H is the column height below the water area, L is the length of the face dimension of the columns, and S is the distance between center columns. The array of four columns was elastically supported by a set of four linear springs to provide low structural damping to the system. Three different section geometries of the columns were tested, namely circular, square, and diamond. Two different current incident angles were tested, 0 and 45°. These configurations of the four-column arrays were selected to cover the range of the main SS – semi-submersible and TLP – tension leg platforms. The aims were to understand the FIM nature of the four-column systems and to provide knowledge to the designers of offshore systems. The range of Reynolds number covered $10{,}000 < Re < 110{,}000$. Concerning the geometry of the columns sections, the amplitude results showed larger amplitudes for the four-column array than the single cylinder case for the circular and diamond cases, in which VIM – vortex-induced motions dominated response was presented. In turn, the amplitudes for the single square case were higher than for the array; in this case, the galloping-dominated response was observed. Concerning the distance between column centers, the amplitude results for the four-column arrays with S/L=3 and 4, were very similar. The four-cylinder array with $S/L = 2$ acted as a single cylinder or changed the wake interference significantly because of the proximity of the columns. Finally, the presence of pontoons had a significant effect on the motions in the transverse direction, and this presence was responsible for decreasing the amplitudes.

1. Introduction

As pointed out by Blevins [1] and Zhao et al. [2], non-symmetric bluff bodies, for example, multi-column systems, are susceptible to two main FIM – flow-induced motions phenomena: VIM – vortex-induced motions, where the frequency of periodic vortex shedding and the frequency of the body oscillation synchronize; and galloping, an aeroelastic instability, caused by changes in the relative angle of attack induced by the body motion resulting in aerodynamic forces in the same degree of freedom as the motion.

In the early 1990s, the offshore industry demanded attention to the VIM phenomena of circular platforms: spar and monocolumn; see review by Fujarra et al. [3], among others. These platforms are characterized by a low aspect ratio ($0.3 < H/L < 6.0$) and a small mass ratio ($m^* < 6$). The VIM due to the high current velocity incidence on circular offshore platforms, in particular cases of spar ($1.5 < H/L < 6.0$) and monocolumn ($0.2 < H/L < 0.5$), reached maximum amplitudes in the transverse direction around 150% of the characteristic diameter of the structures and cause fatigue life decreased by about 30% in the mooring and riser systems. For example, Dijk et al. [4], Irani & Finn [5] and Roddier et al. [6] presented studies on the VIM of spar platforms and amplitudes in the transverse directions around one diameter were observed; moreover, Sagrilo et al. [7], Gonçalves et al. [8] and Saito et al. [9] detailed studies on VIM of monocolumn platforms,

* Corresponding author.
E-mail addresses: goncalves@edu.k.u-tokyo.ac.jp (R.T. Gonçalves), nhepp@equinor.com (N.H. Hannes), mariaefchame@usp.br (M.E.F. Chame), pedropaludetto@usp.br (P.P.S.P. Lopes), hirabayashi@k.u-tokyo.ac.jp (S. Hirabayashi), suzukih@sys.t.u-tokyo.ac.jp (H. Suzuki).

https://doi.org/10.1016/j.apor.2019.102019
Received 25 February 2019; Received in revised form 26 September 2019; Accepted 8 December 2019

Nomenclature

A_x	characteristic amplitude in the in-line direction
A_y	characteristic amplitude in the transverse direction
A_{yaw}	characteristic amplitude for the yaw motions
D	column characteristic dimension due to the current incidence angle
GM	metacentric height
H	column height below the water line
H_m	vertical position of the mooring line fairleads
H_t	height of the water level of the towing tank
H/L	columns aspect ratio
K	individual stiffness constant for a spring
K_x	total stiffness of the system in the in-line direction
K_y	total stiffness of the system in the transverse direction
K_{yaw}	total rotational stiffness of the system for yaw motion
KG	distance between the center of gravity and the base
L	length of the face dimension of the columns
L_0	natural length of the spring
L_m	in-line position of the mooring line fairleads
L_t	length of the towing tank
m	mass
m^*	mass ratio
R_{XX}	radius of gyration around the X axis
R_{YY}	radius of gyration around the Y axis
R_{ZZ}	radius of gyration around the Z axis
Re	Reynolds number
S	distance between column centers
St	Strouhal number
$S/$	distance between columns ratio
T_{0x}	natural period of the motion in the in-line direction in still water
T_{0y}	natural period of the motion in the transverse direction in still water
T_{0yaw}	natural period of the yaw motion in still water
U	current velocity
V_r	reduced velocity
W_m	transverse position of the mooring line fairleads
W_t	width of the towing tank
X	in-line direction
Y	transverse direction
Z	vertical direction
ρ	fluid density
θ	current incidence angle
$\varnothing_m$	diameter of the ring for the mooring line fairleads

Abbreviation

CFD	computational fluid dynamics
DD	deep-draft semi-submersible platform
DOF	degree of freedom
FIM	flow-induced motions
FOWT	floating offshore wind turbine
PSD	power spectrum density
SS	semi-submersible platform
std	standard deviation
VIM	vortex-induced motions

in which maximum amplitudes in the transverse direction around 150% of the diameter were observed with a large couple with the motion in the in-line direction.

Works about fundamental VIM of low aspect ratio circular cylinders are few in the literature; among which Rahman & Thiagarajan [10], Zhao & Cheng [11] and Gonçalves et al. [12] can be highlighted.

Rahman and Thiagarajan [10] performed model tests for 1 DOF – degree of freedom (transverse direction) VIM, mass ratio equal to 1.6, and aspect ratio ranging from 0.5 up to 13. The maximum amplitudes observed were 1.2D with the presence of the lower branch for high values of reduced velocity. The authors concluded that a decrease in the aspect ratio was responsible for a reduction of the amplitudes in the transverse direction.

Zhao and Cheng [11] performed CFD simulations for 1 DOF VIM, mass ratio equal to 2, and aspect ratio ranging from 1 up to 20. The objective was to understand the 3D structures around the cylinder free end. The vortices that were shed from the cylinder with aspect ratio lower than 2 were found to be generated from the cylinder free end and convected toward the top end of the cylinder by the up-wash velocity.

Gonçalves et al. [12] presented a series of fundamental results of 2 DOF VIM of floating circular cylinders and aspect ratio ranging from 0.3 up to 2. The amplitude results showed a decrease in amplitude with decreasing aspect ratio in the in-line and the transverse directions. The frequency results confirm a different behavior for cylinders with aspect ratio lower than 0.5; in these cases, the cylinder free-end effects were predominant. The resonant behavior was no longer observed for aspect ratio lower than 0.2. The decrease in Strouhal number with decreasing aspect ratio is also verified, as well as for drag and lift forces. The amplitude results for the vertical direction, roll, pitch, and yaw did not affect the FIM behavior.

Gonçalves et al. [13] and Gonçalves et al. [14] presented results for low aspect ratio square cylinders with 0 and 45-deg incidences and showed the different behavior for the cylinders with square and circular sections with low aspect ratio. The studies allowed conjecturing that the FIM for square cylinders with 0-degree incidence was more similar to the galloping phenomenon. However, for the square section cylinder with 45-degree incidence, the behavior was more similar to the VIM phenomenon than in the circular section cylinder case. The same statements can be found in Zhao et al. [2] for long cylinders with square sections.

The VIM has also been studied on the multi-column platform, such as SS semi-submersible platforms, TLP – tension-leg platforms, and FOWT – floating offshore wind turbines; an overview of VIM of multi-column floaters can be found in Irani et al. [15]. As highlighted by Waals et al. [16], Gonçalves et al. [17], and Lamas et al. [18], the multi-column platforms were susceptible to VIM and galloping phenomena.

Gonçalves et al. [19] present a comparison between VIM results for four-circular and four-square column sections. The circular columns seemed to result in higher VIM response in the transverse direction for all current headings compared with the square columns, which is important to consider in the design stage of the semi-submersible.

Liu et al. [20] carried out experiments of four-square columns and four-diamond columns, aiming to examine the influence of the column configuration. Diamond configurations showed a similar trend and similar peak values in the transverse response for 0 and 45-deg incidences, and the transverse response was dominated by the vortex-induced motions. Square configurations showed a similar trend and similar peak values in the transverse response for 0 and 45-deg incidences, and the transverse response was lower than diamond cases.

Ramirez and Fernandes [21] performed VIM model tests for a TLP platform with four-diamond columns, and observed an increase in the yaw response with the current speed, confirmed the galloping behavior for this particular geometry.

In summary, all the works showed that the VIM response was profoundly impacted by the column section geometry, as well as by the incidence angle of the current.

The previous studies about VIM focused on the final geometry of the offshore platforms with four columns. The works presented results with

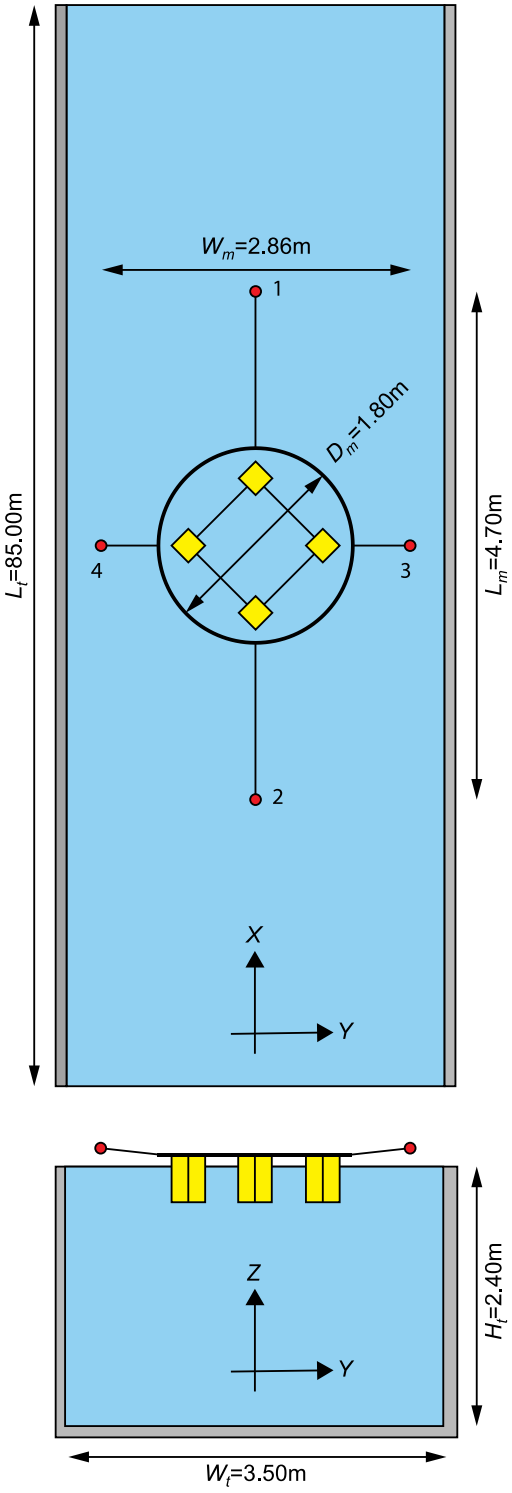

Fig. 1. Schematic of the simplified mooring system setup composed of four spring lines at the towing tank.

the presence of pontoons as well. For a better understanding of the behavior of the multi-column system, fundamental studies are necessary, i.e., simple geometries.

Fundamental studies on understanding the flow around a fixed array of cylinders with low aspect ratio can be found in Liu et al. [22], Gonçalves et al. [23] and Gonçalves et al. [24].

Liu et al. [22] performed a range of experimental and CFD – computational fluid dynamics studies on the flow characteristics around four circular section cylinders in a square configuration covering three

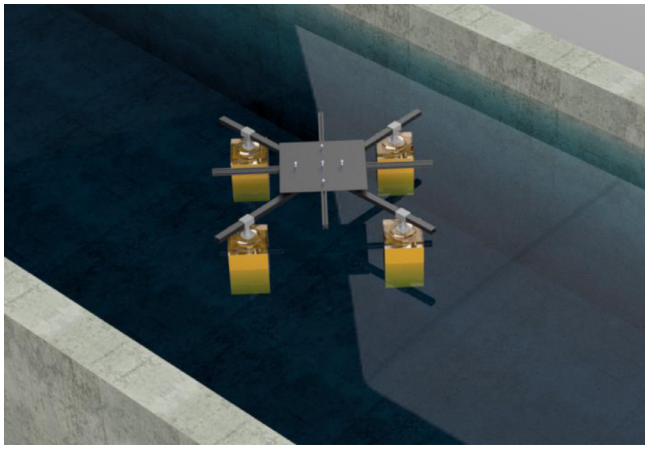

Fig. 2. Schematic of the 4-column model in the towing tank.

different spacing ratios from 3.45 up to 5.17, and four different incidence angles ranging from 0° up to 45° The mean drag force was large for the upstream cylinders, and similar flow patterns were observed for the spacing ratio studied. The shear layers and its interferences may be responsible for the VIM behavior for the free condition due to a recognizable dominant frequency.

Gonçalves et al. [23] and Gonçalves et al. [24] carried out experiments on the flow around a stationary array of four cylinders with low aspect ratio equal to 1.5, and spacing ration ranging from 2 up to 4. Three different column section geometries namely, circular, square and diamond; and three conditions of current incidence angle, 0, 22.5, and 45° were tested. Regarding the columns section, the lift force results for the whole system showed that the section of the columns was responsible for the predominant flow behavior around the multi-column systems instead of the wake interference due to the column position. Moreover, the flow behavior was different for spacing ratio equal to 2, in which the array of cylinders acted as a unique body with a large characteristic diameter.

Trying to understand the FIM on the fundamental way, Gonçalves et al. [25] performed FIM experiments of 3-column platforms and showed the source of the motions could be due to VIM-dominated response or to the galloping behavior.

In this context, the aims were to understand the FIM of 4-column platform without the presence of pontoons by fundamental experiments in a towing tank. The effect of the geometry of the column sections (circular, square, and diamond) and the distance between column centers (S/L= 2, 3 and 4) on the FIM were evaluated.

1.1. Experimental setup

All the experiments were carried out in a towing tank at the University of Tokyo, Tokyo, Japan. The dimension of the test section is 85.0 m x 3.5 m x 2.4 m (length x wide x depth).

Fig. 1 shows the sketch of the setup on the towing carriage. Fig. 2 presents a schematic of the four-diamond-column case with the 45-deg incidence in the towing tank.

The circular column models were made of acrylic with external diameter $D = L$=250 mm, as well as the square (diamond) column models with face dimension L=220 mm. The columns did not present a roughness level and may be considered smooth cylinders. The aspect ratio of the columns was $H/L = 1.5$, the typical value for SS. The models were floating; thus, the value of the mass ratio, m^*, was equal to one.

A crossbar was designed to support the four-column array. The support allowed quickly changing the column geometry and distance between column centers. The deck configuration allowed for changes in the current incident angle, keeping the same initial restoring force. An isometric view of the models can be seen in Fig. 3. The model properties

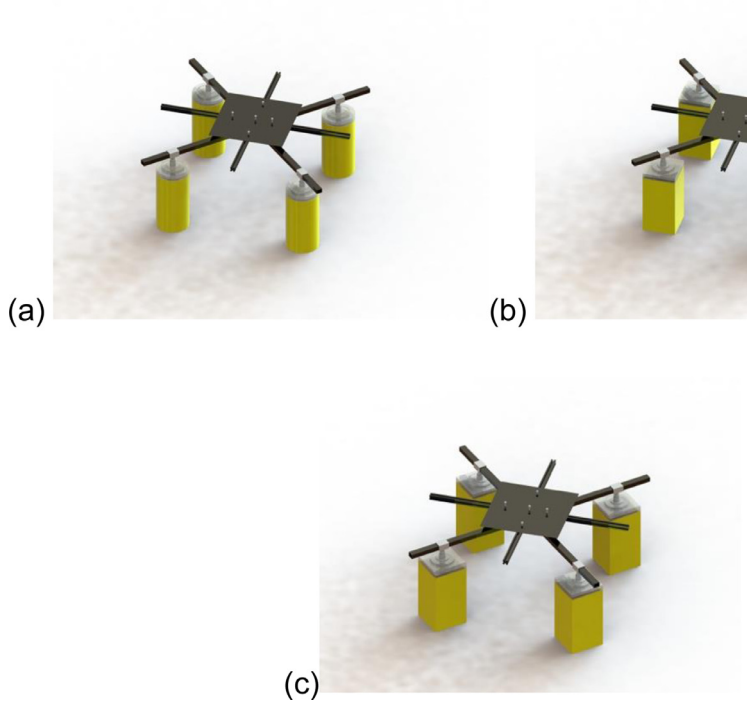

Fig. 3. Isometric view of the 4-column models with cross-bar: (a) circular, (b) square and, (c) diamond.

Table. 1
Inertia properties of the four-column models with 0-deg incidence.

Property	Circular			Square/Diamond		
S/L	2	3	4	2	3	4
m [kg]	73.2	73.2	73.2	63.9	63.9	63.9
KG [mm]	248.4	248.4	248.4	254.3	254.3	254.3
GM [mm]	117.4	575.2	868.8	71.6	511.4	771.4
R_{XX} [mm]	377.3	453.6	542.7	382.8	450.9	528.1
R_{YY} [mm]	372.9	447.9	536.1	382.8	450.9	528.1
R_{ZZ} [mm]	411.2	542.3	685.4	451.0	562.9	684.2
T_{0x} [s]	13.8	13.9	13.8	14.2	14.8	14.0
T_{0y} [s]	14.5	14.5	14.4	14.5	14.3	14.4
T_{0yaw} [s]	4.4	6.2	7.9	3.9	5.5	7.0

Table. 2
Individual spring characteristics.

Spring number	*K* [N/m]	L_0 [mm]	Pre-tension[N]
1	8.0	200	7.0
2	8.0	200	7.0
3	9.7	230	2.9
4	9.7	230	2.9

Table. 3
Stiffness properties in function of the mean offset.

Offset X [mm]	K_x [N/m]	K_y [N/m]	K_{yaw} [N.m/°]
0	28.9	27.2	0.31
100	29.3	26.6	0.31
200	30.4	25.6	0.31
300	31.7	24.8	0.32
400	33.0	24.2	0.32
500	34.1	23.7	0.33

can be seen in Table 1.

The dimensions of the simplified mooring system setup composed of four springs connected to the towing car are presented in Fig. 1. The

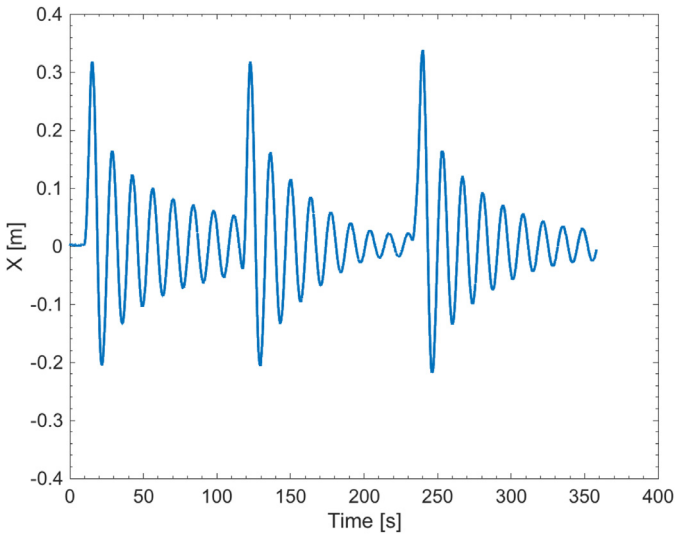

Fig. 4. Time series of a decay test in the in-line direction for the array of circular cylinders with S/L = 4.

individual characteristics of each spring, namely stiffness constant, K, the natural length of the spring, L_0, and pre-tension are presented in Table 2. The dimensions of the mooring system, as in Fig. 1, together with the spring characteristics, as in Table 2, are responsible for the total stiffness of the system. The total stiffness of the system in the in-line direction, K_x, and in the transverse direction, K_y, as well as the rotational stiffness in the vertical direction, K_{yaw}, was calculated applying the analytical formulation by Pesce et al. [26] for different values of mean offset position. Displacements around the mean offset conditions around 0.5 L, 1.5 L and 10° were applied in the in-line direction, the transverse direction and yaw according, respectively, as observed in the experiments. The maximum offset condition observed for the highest reduced velocity was 500 mm. These values were used to calculate the total stiffness values, as presented in Table 3.

The maximum difference in the stiffness value in the in-line and in

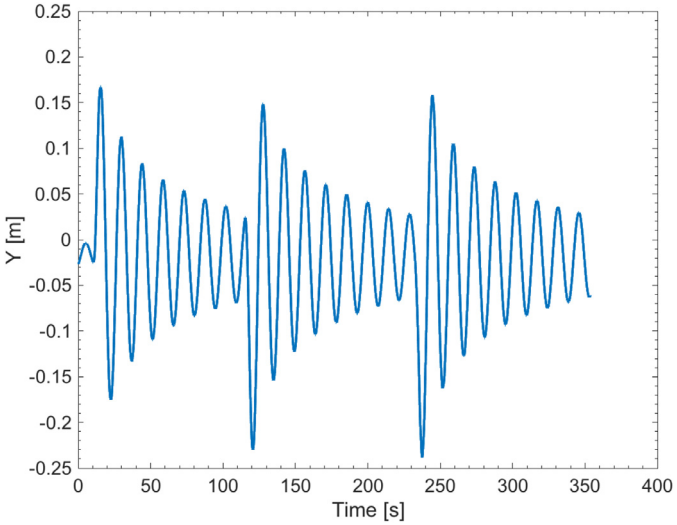

Fig. 5. Time series of a decay test in the in-line direction for the array of circular cylinders with $S/L = 4$.

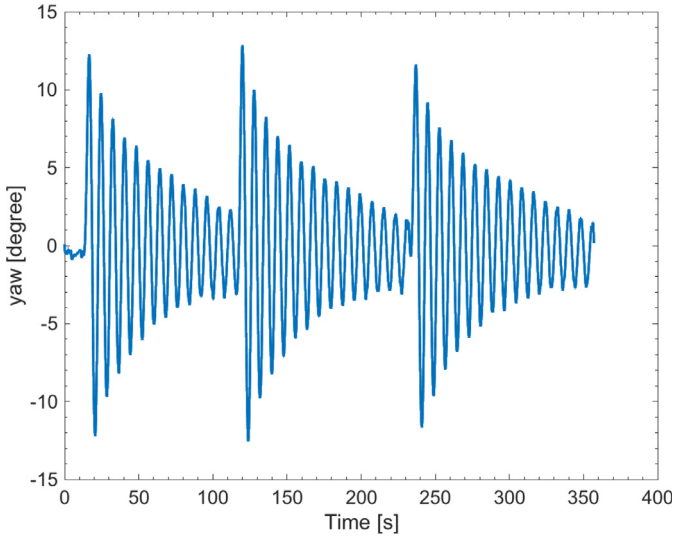

Fig. 6. Time series of a decay test for yaw motions for the array of circular cylinders with $S/L = 4$.

the transverse direction due to the mean offset was 18% for 500 mm offset that occurred for highest reduced velocities. For the range of reduced velocities lower than 10, i.e., mean offset lower than 300 mm, the difference was 9%. The natural period may not significantly affect by the offset position. Therefore, the results are discussed using the reduced velocity calculated with the natural period in still water in the initial equilibrium position. The rotational stiffness in the yaw direction was not affected by the offset position.

The structural damping was very low around $\zeta = 2\%$ calculated for each spring by decay tests in the air.

The 6 DOF motions data was acquired along 70 m in the towing tank with the sampling frequency of 30 Hz using an optical motion capture system.

Sixteen different configurations were tested, namely: circular, square and diamond cylinders; three different distances between columns $S/L = 2$, 3 and 4; and two different angles of the current incidence, namely $\theta = 0$ and 45°.

The experiments were performed at for least 15 different current velocities for each configuration, and the Reynolds number range was $10,000 < Re < 110,000$. The Reynolds number was calculated using the value D. The maximum velocity of the towing car was around 0.4 m/s.

For all the cases, decay tests in still water were performed to calculate the natural frequency for the 6DOF. At least three repetitions of decay tests were conducted, and at least 6 cycles were used for better statistic results, see results in Table 1. Examples of the times series of decay tests in the in-line, transverse, and yaw are presented in Fig. 4, Fig. 5 and Fig. 6, respectively.

Figs. 7 and 8 show the configuration tested. Table 4 presents details about the configurations tested.

2. Analysis methodology

2.1. Motion amplitudes

The FIM response of the models was analyzed through the std – Standard Deviation of displacements in the transverse direction, in the in-line direction and angles of rotation in the case of the yaw motion. The std was calculated in the case of a set of n values (x_1, x_2, ...,x_n) as:

$$x_{std} = \sqrt{\frac{1}{n-1}\sum_{i=1}^{n}(x_i - \bar{x})^2} \tag{1}$$

Moreover, as commonly found, nominal non-dimensional amplitudes for the motions in the transverse and in-line directions were presented as a quotient of the standard deviation of the displacements times $\sqrt{2}$ by the face dimension of the column A_y/L and A_x/L, respectively, as:

$$\frac{A_y}{L} = \sqrt{2}\frac{y_{std}}{L} \tag{2}$$

$$\frac{A_x}{L} = \sqrt{2}\frac{x_{std}}{L} \tag{3}$$

For the angles of yaw, A_{yaw}, no dimensionless presentation was adopted, as usual in the literature, as:

$$A_{yaw} = \sqrt{2}yaw_{std} \tag{4}$$

2.2. Characteristic motion frequency

The characteristic motion frequency was calculated for the motions in the transverse direction, f_y. The characteristic motion frequency was defined as the peak of the highest energy level in the PSD – power spectrum density. The results will be presented in the non-dimensional form using the natural frequency of the motion in the transverse direction in still water, i.e., f_y/f_{0y}.

2.3. Reduced velocities

Reduced velocity V_r was defined as a function of the incident current velocity, U, the natural period of motion in the transverse direction in still water, T_{0y}, and the characteristic length of the body section subjected to a vortex shedding, D.

$$\boldsymbol{V_r} = \frac{\boldsymbol{U}.\boldsymbol{T_{0y}}}{\boldsymbol{D}} \tag{5}$$

In this case, D can be written as a function of the current incidence angle for square columns, to better represent the characteristic length of the column section on the flow, i.e., $D = L(|sin\theta| + |cos\theta|)$, where θ is the current incidence angle. For circular columns cases $D = L$ for all incidence angles.

3. Experimental results

The spacing ratio $S/L = 4$ is the typical value among the SS platforms in the offshore scenario, and because of that, it was chosen to be

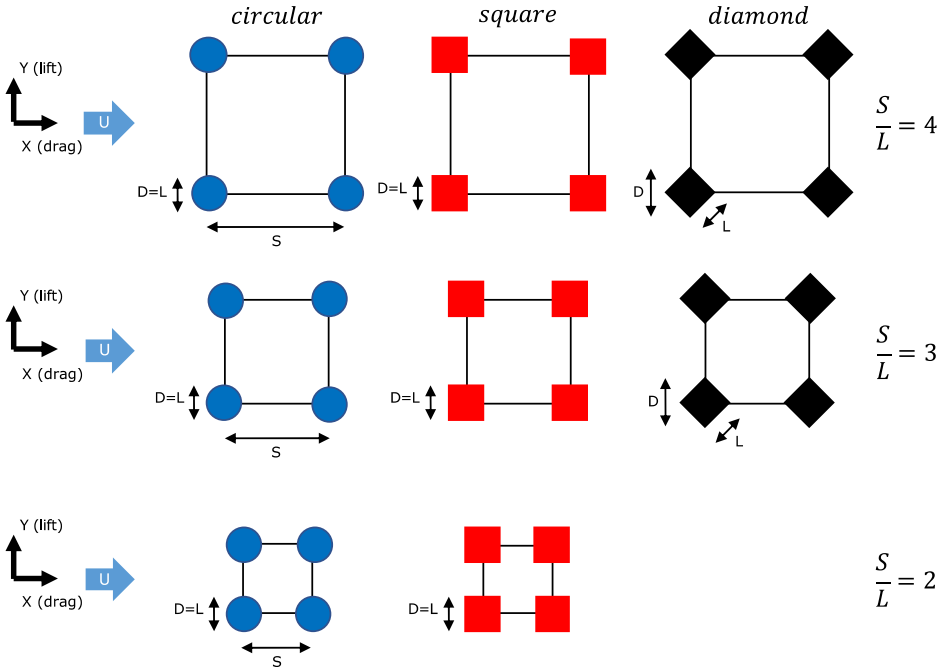

Fig. 7. Sketch of the 4-column models for 0-deg incidence with different column section geometries (from right to left: circular, square and diamond) and different spacing ratios (from top to bottom: S/L = 4, 3 and 2).

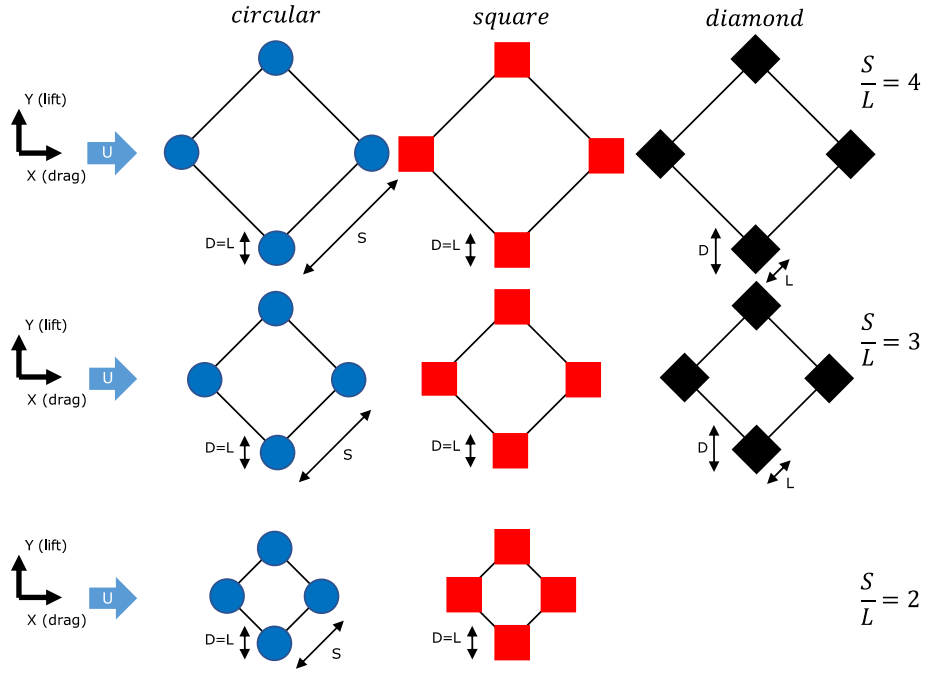

Fig. 8. Sketch of the 4-column models for 45-deg incidence with different column section geometries (from right to left: circular, square and diamond) and different spacing ratios (from top to bottom: S/L = 4, 3 and 2).

the main case. Figs. 9–11 present the characteristic amplitudes for the 4-cylinder arrays with $S/L = 4$, $\theta = 0$ and 45°, and different column geometries.

The results showed a considerable difference due to the column section geometry for $S/L = 4$. The amplitudes were the largest for the circular column cases for all the degrees of freedom, namely, in-line, transverse and yaw. Only for the amplitudes in the transverse direction, the results for circular and diamond cases were comparable for $V_r < 6$.

The amplitudes in the transverse direction, Fig. 9, showed the effect of the column section geometry.

The amplitudes in the transverse direction presented a local maximum only for the diamond column case, around $V_r = 7$, and a decrease in the amplitudes next. This behavior is similar to the VIM phenomenon due to the presence of the resonance and desynchronization ranges. In turn, a decrease in amplitudes was not observed when increasing the reduced velocities for the circular and square column cases.

A behavior similar to galloping can be observed for the square column cases due to the almost linear increase in the amplitudes when increasing the reduced velocity. High values of reduced velocities were performed for the square column case, and no drop in the amplitudes

Table. 4
Matrix of conditions carried out for FIM studies of the 4-column models.

Cylinder section geometry	θ [deg]	L [mm]	D [mm]	H/L	S/L	Re [x 10^3]
Circular	0	250	250	1.5	2, 3, 4	15 – 65
Circular	45	250	250	1.5	2, 3, 4	15 – 65
Square	0	220	220	1.5	2, 3, 4	10 – 100
Square	45	220	220	1.5	2, 3, 4	10 – 100
Diamond	0	220	311	1.5	3, 4	25 – 110
Diamond	45	220	311	1.5	3, 4	25 – 110

was verified, and the galloping behavior may be confirmed. However, it may not be confirmed for the circular column cases due to the limitation in the reduced velocity tested, $V_r < 10$.

Resonance peak for long aspect ratio cylinders, $L/D > 13$, and 1 DOF, is typically around reduced velocities 5 and 7, as in Williamson and Govardhan [27]; the higher value for the VIM behavior, peaks for $V_r > 7$ or absence of peak, is due to the low aspect ratio characteristics, $L/D < 2$, small mass ratio, $m^* = 1$, and 6DOF, as discussed by Gonçalves et al. [12].

Concerning the incidence angles, differences in the amplitudes in the transverse direction, Fig. 9, were observed for the square and diamond cases for the reduced velocities larger than 10 and 7, respectively, when comparing 0 and 45-deg incidences. No difference was observed for the circular cases. The maximum values of the amplitudes in the transverse direction for $S/L = 4$ were A_y/L=1.25, 0.95 and 0.80 for the circular, square, and diamond cases, respectively.

For the amplitudes in the in-line direction, Fig. 10, the results of the amplitude showed a local maximum for the circular and diamond cases, around $V_r = 3.5$, which represent the resonance of the motion in the in-line direction and its double frequency characteristic, similarly to the FIM phenomenon. The same behavior could not be verified for the square cases. Yet the increase in the amplitudes with increasing reduced velocity for the square column cases may be considered a galloping phenomenon.

Concerning the incidence angles, the amplitudes in the in-line direction, Fig. 10, were significantly different only for the square cases in the range of $V_r > 10$. The maximum values of the amplitudes in the in-line, Fig. 10, for $S/L = 4$, were A_x/L=0.45, 0.30 and 0.15 for the circular, square, and diamond cases, respectively.

The results of the amplitudes of yaw motion, Fig. 11, were more dispersed than for other degrees of freedom. For the square geometry, the yaw motion increased with the increase of reduced velocity

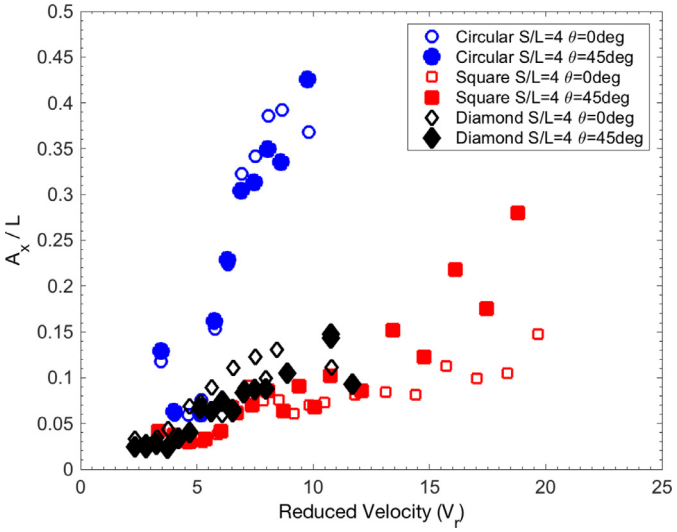

Fig. 10. Nondimensional amplitudes for the motions in the in-line direction for the array of cylinders with S/L = 4.

similarly to the galloping behavior. For the circular and diamond cases, the presence of a maximum local could be explained by a VIM behavior, but it is not possible to confirm only with these results. Since the ratio between the natural periods of the motions in the transverse direction and yaw was T_{0y}/T_{0yaw}≅1.8, a resonance of the yaw motion was expected to occur around a reduced velocity 1.8 times higher than the resonance of the motion in the transverse direction; however, the resonance was not observed in that range. More studies need to be conducted for the yaw motion to understand the source of the FIM.

For the yaw motions, Fig. 11, the incidence angle affected the results significantly. The results of yaw amplitudes for 45-deg incidence were higher compared to the ones for 0-deg incidence. The position of the columns and how it interfered with the wake was responsible for affecting the moments of yaw and phase of the forces in each column. This behavior was not crucial for the motions in the transverse and in-line direction due to the large spacing ratio, $S/L = 4$. The maximum values of the amplitudes of the yaw motions for $S/L = 4$ were A_{yaw}= 4.5, 5.5 and 7.0° for the circular, square and diamond cases, respectively, and occurred for the 45-deg incidence.

Two most common galloping analyses discussed in the literature are: the quasi-steady dynamics, i.e., the fluid force on the structure is

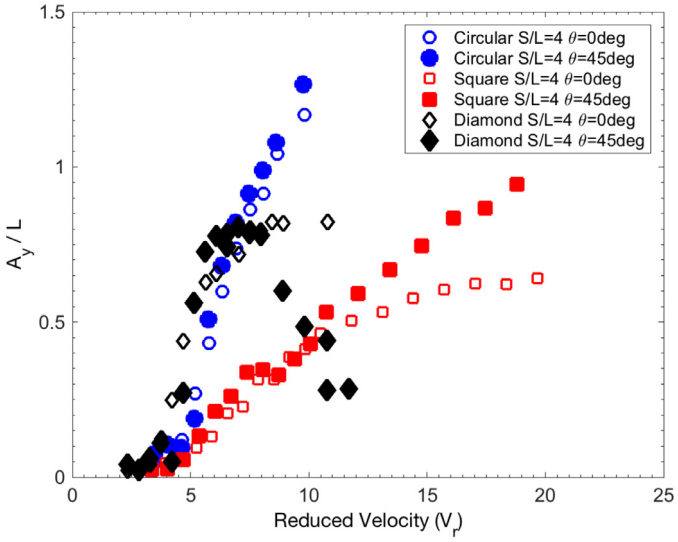

Fig. 9. Nondimensional amplitudes for the motions in the transverse direction for the array of cylinders with S/L = 4.

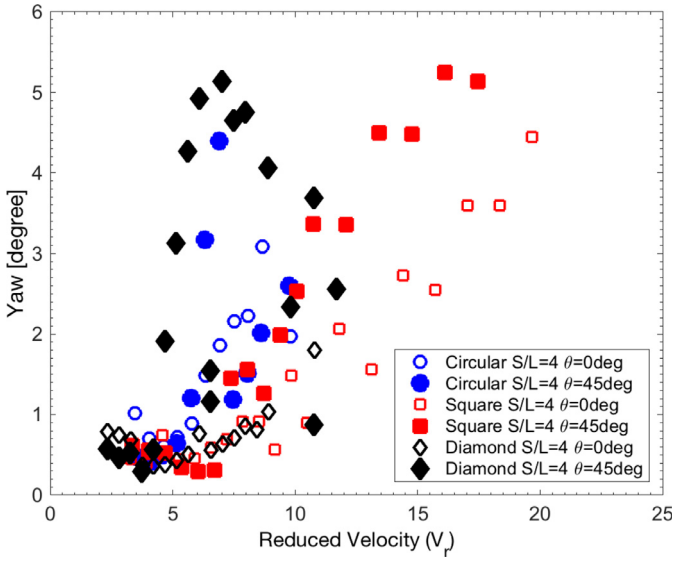

Fig. 11. Yaw motion amplitudes for the array of cylinders with S/L = 4.

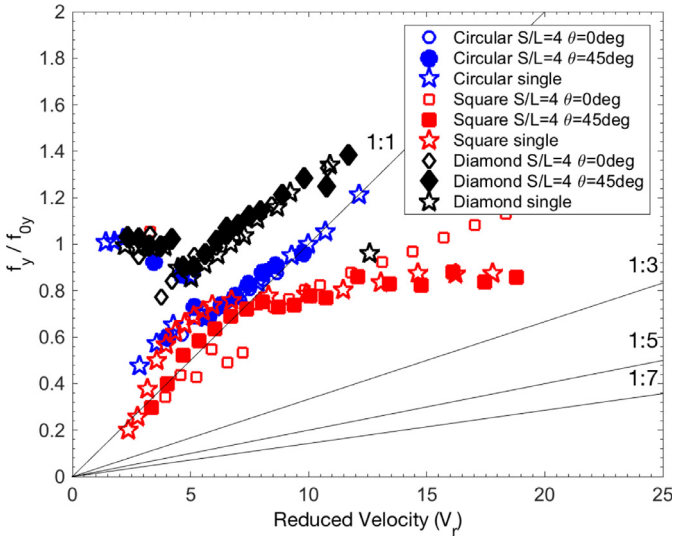

Fig. 12. Nondimensional frequency for the motions in the transverse direction for the array of cylinders with S/L = 4.

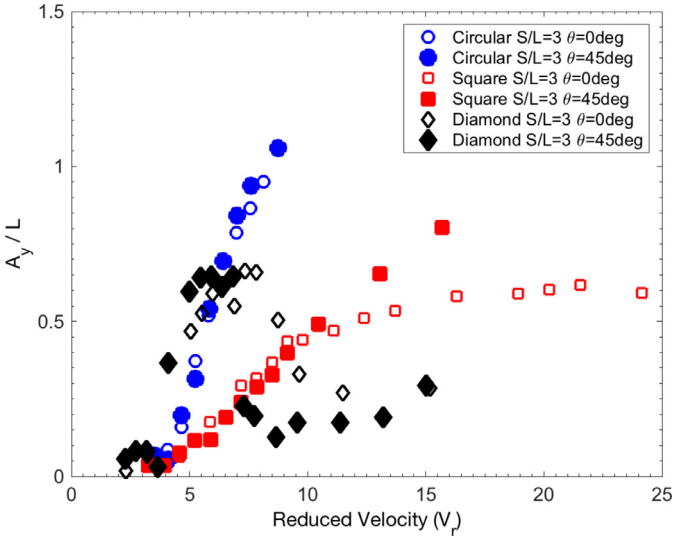

Fig. 13. Nondimensional amplitudes for the motions in the transverse direction for the array of cylinders with S/L = 3.

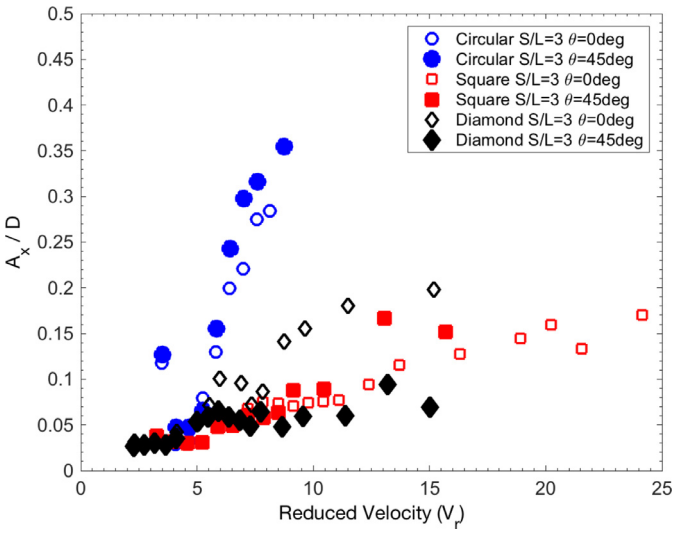

Fig. 14. Nondimensional amplitudes for the motions in the in-line direction for the array of cylinders with S/L = 3.

assumed to be determined solely by the instantaneous relative velocity, so the fluid forces can be measured on stationary models held at various angles, as discussed by Blevins [1]; and, the frequency component analysis, i.e., the frequencies of the motion and the lift force are compared to determine the kinks of galloping regime, as detailed by Zhao et al. [2]. In our work, fluid forces were not measured on a stationary model, but the frequency analysis for the motions in the transverse direction can be evaluated, and the methodology by Zhao et al. [2] can be applied.

Fig. 12 presents the nondimensional frequency for the array of 4-cylinders with $S/L = 4$, $\theta = 0$ and 45°, and different column geometries. The results of a single cylinder from Gonçalves et al. [28] were included to corroborate the discussion.

The Strouhal number for circular and square cylinders with low aspect ratio, $H/D = 1.5$, undergoing VIM is around $St = 0.1$, as presented in Gonçalves et al. [13] and Gonçalves et al. [12]. For circular and diamond cases, it was possible to observe that the results of f_y/f_{0y} followed the 1:1 synchronization regime line, $St = 0.1$; thus, VIM-dominated response can be confirmed, where the motion frequency, f_y, and vortex-shedding frequency, f_s, synchronize, and the motion was mostly periodic and regular. For square cases, the results followed the 1:1 synchronization for the range of $V_r < 8$ and changed the slope to 1:3 and 1:7 synchronizations for 0-deg and 45-deg, respectively. These behaviors confirmed that the FIM of 4-square columns were predominant VIM for $V_r < 8$; and galloping for high reduced velocities, because the vortex-shedding frequency was 3 and 7 times higher than the frequency of the motion. The methodology using the characteristic frequencies and the motions in the transverse direction showed that the source of the FIM phenomenon of 4-column arrays with $S/L = 4$ is the same as for the single cylinders, i.e., VIM-dominated response for circular and square columns, and galloping-dominated response for square columns and high reduced velocities. The same statements for single cylinders were previously discussed in details by Zhao et al. [2] and contributed to validating the results here presented.

Figs. 13–15 present the characteristic amplitudes for the 4-cylinder arrays with $S/L = 3$, $\theta = 0$ and 45°, and different column geometries. In general, the results for $S/L = 3$ presented the same behavior as those for $S/L = 4$.

The column geometry affected the results in the transverse direction, as in Fig. 13. For the square column cases, a behavior similar to

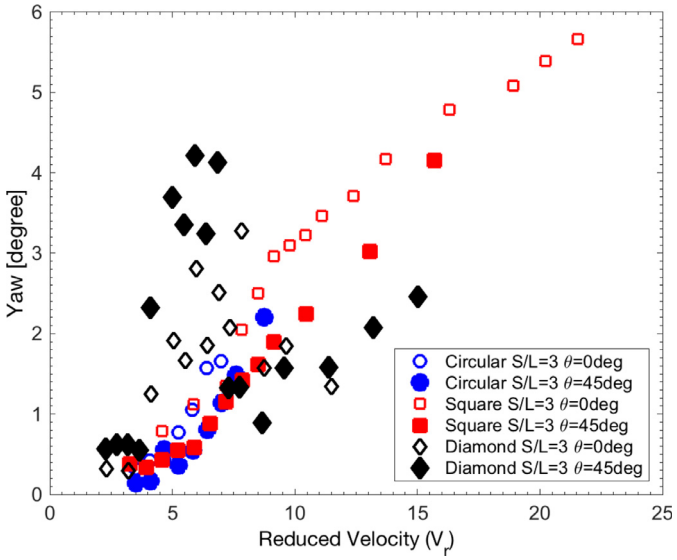

Fig. 15. Yaw motion amplitudes for the array of cylinders with S/L = 3.

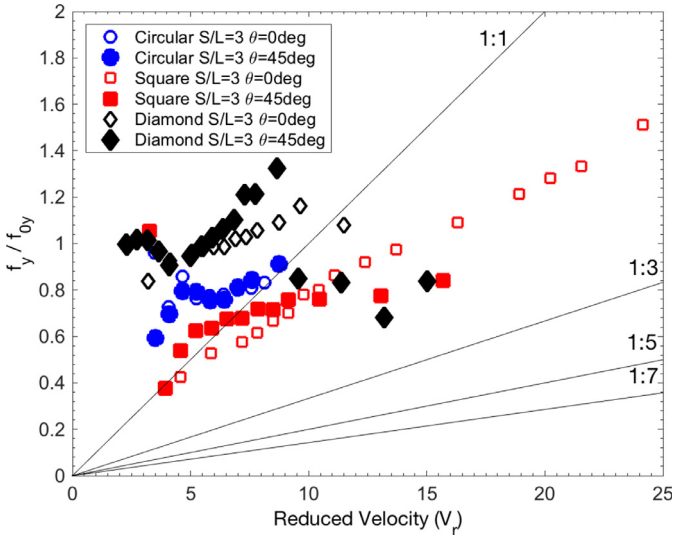

Fig. 16. Nondimensional frequency for the motions in the transverse direction for the array of cylinders with S/L = 3.

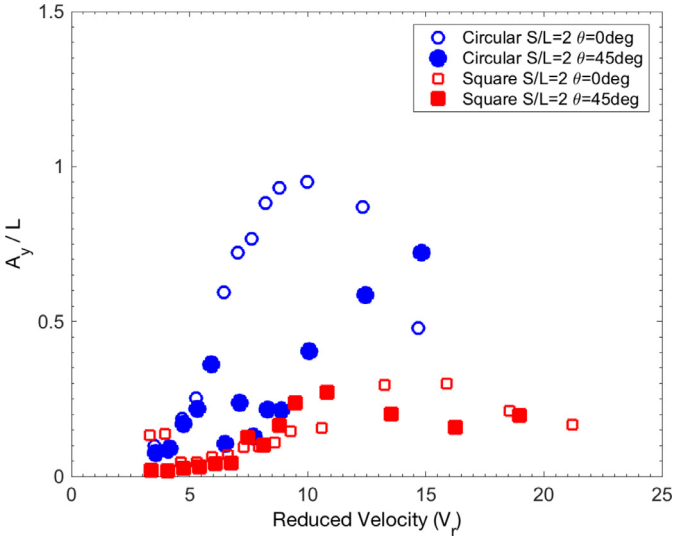

Fig. 17. Nondimensional amplitudes for the motions in the transverse direction for the array of cylinders with S/L = 2.

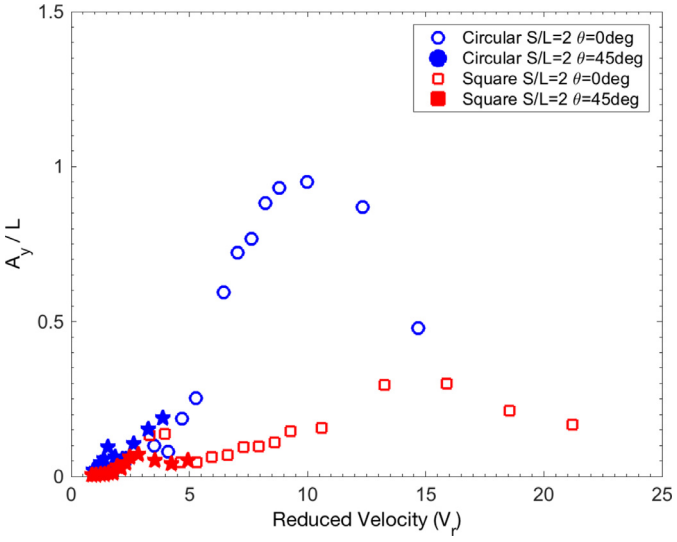

Fig. 18. Nondimensional amplitudes for the motions in the transverse direction for the array of cylinders with S/L = 2 with the reduced velocity adjustment to the single body projected face.

galloping with an increase in the amplitude by increasing the reduced velocity can be observed. For the circular cases, the VIM behavior could not be confirmed only by the motions in the transverse direction, due to the absence of the desynchronization range and low reduced velocities range tested; in turn, for the diamond cases, the VIM can be observed because the presence of a maximum amplitude and a desynchronization range characterized by the drop of amplitudes. The maximum values of the amplitudes in the transverse direction for $S/L = 3$ were A_y/L=1.05, 0.80 and 0.65 for the circular, square, and diamond cases, respectively.

Concerning the incidence angle, the effect of the wake interference is more significant for $S/L = 3$ than for $S/L = 4$ due to the proximity of the cylinders. For the cases of square and diamond cylinders, the wake was more significant due to the fixed separation point than for the circular cases. The distance between cylinders was smaller for the diamond cases with 45-deg incidence than the other ones; consequently, the wake around the cylinders was more affected, and thus the synchronization range changed when comparing 0 and 45-deg incidences, see Fig. 13.

The amplitudes for the motions in the in-line direction were more affected by the incidence angle for the diamond cases. Again, the explanation was the proximity of the columns for these cases, which probably started to impact the flow in the region inside the columns. For diamond cases with 45-deg incidence, a region with a dead zone (low flow interactions) could be observed. The values of the amplitudes in the in-line, Fig. 14, for $S/L = 3$, were A_x/L=0.35, 0.15 and 0.20 for the circular, square, and diamond cases, respectively.

The amplitudes of the yaw motions for $S/L = 3$ are presented in Fig. 15. The results were more dispersed than for $S/L = 4$, confirming the more considerable wake interference for this column spacing ratio. The amplitude results of yaw motion showed the galloping behavior for the square cases, as for $S/L = 4$. The yaw motion could not be considered a VIM phenomenon for the diamond case only due to the presence of a maximum and subsequent decrease of amplitudes, because the resonance frequency did not match the natural frequency of yaw, as explained for the $S/L = 4$ cases. For the circular cases, it was not possible to observe a peak in the yaw amplitudes differently from $S/L = 4$; thus, it was not possible to determine the nature of the FIM phenomenon for the circular cases due to the small range of reduced velocities tested.

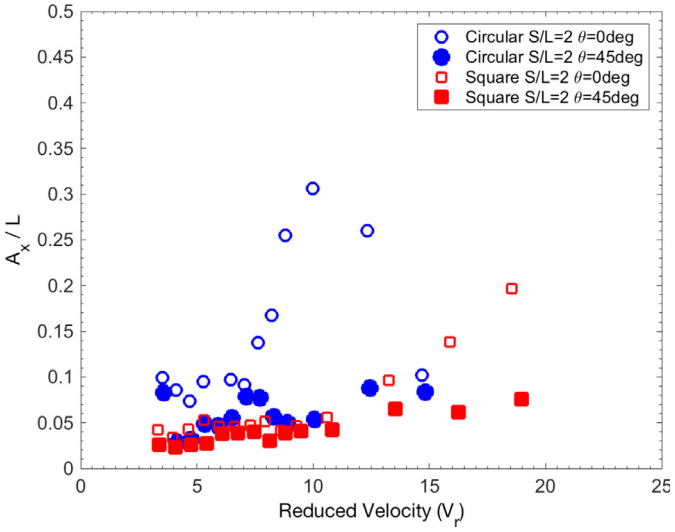

Fig. 19. Nondimensional amplitudes for the motions in the in-line direction for the array of cylinders with S/L = 2.

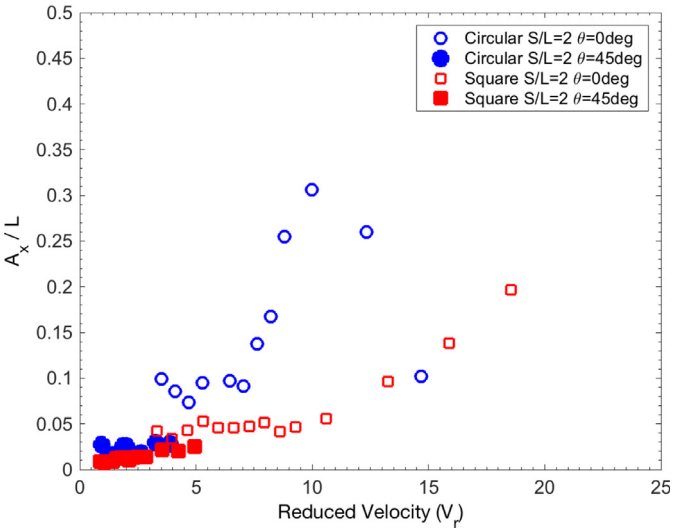

Fig. 20. Nondimensional amplitudes for the motions in the in-line direction for the array of cylinders with S/L = 2 with the reduced velocity adjustment to the single body projected face.

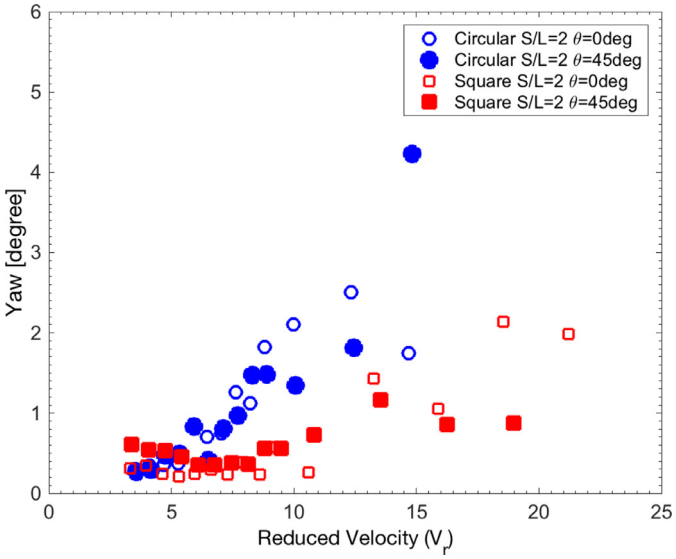

Fig. 21. Yaw motion amplitudes for the array of cylinders with S/L = 2.

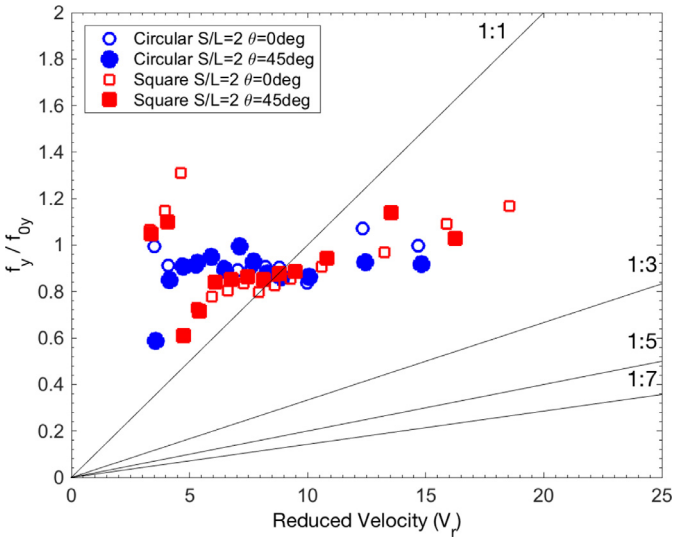

Fig. 22. Nondimensional frequency for the motions in the transverse direction for the array of cylinders with S/L = 2.

The maximum values of the amplitudes of the yaw motions for $S/L = 3$ were A_{yaw}= 2.2, 5.7 and 4.2° for the circular, square and diamond cases, respectively.

Fig. 16 presents the nondimensional frequency for the array of 4-cylinders with $S/L = 3$, $\theta = 0$ and 45°, and different column geometries. As in the results for $S/L = 4$, the characteristic frequency and motion amplitudes in the transverse direction together can be used to confirm the FIM source for each case. The circular and diamond cases followed the 1:1 synchronization regime confirming the VIM-dominated response; the diamond case did not follow the 1:1 line after the drop in the amplitudes, as expected for vortex shedding dominated phenomenon. For square cases, the small range of reduced velocity followed the 1:1 synchronization regime, around the natural frequency of the system, and changed to higher synchronization regimes 1:3, 1:5 or 1:7 as expected for a galloping phenomenon. These statements confirmed the same behavior presented for $S/L = 4$ and confirmed that the column section geometry was responsible for the FIM source and not the incidence angle.

Figs. 17, 19, and 21 present the characteristic amplitudes for the 4-cylinder arrays with $S/L = 2$, $\theta = 0$ and 45°, and different column geometries. Only experiments for circular and square columns were performed for $S/L = 2$ due to the limitation in the experimental setup. The results showed a significant difference due to the column section geometry for $S/L = 2$, and the results were very different when compared to larger spacing ratios, as presented before.

The incidence angle affected the amplitude significantly in the transverse direction for $S/L = 2$, see Fig. 17. The most considerable differences were observed for the circular case. The explanation may be that the wake interference acted as a unique body for $S/L = 2$ and 45-deg incidence, i.e., the flow around the array visualizes a single body with a characteristic length of $D = (2\sqrt{2} + 1)L$. Yet, for 0-deg incidence, the flow was able to go inside the array of the cylinders, and the wake could be developed for each cylinder individually, and no modifications were needed. Applying these assumptions, the reduced velocity was calculated using the new value of the characteristic length, and nondimensional amplitudes were calculated using $D = 3L$; the results are presented in Fig. 18. The new amplitude results were quite similar now for the 0 and 45-deg incidences. It is essential to highlight that these assumptions did not consider the changes in the aspect ratio, H/L, and the new range of reduced velocities, $1 < V_r < 5$, is narrow to

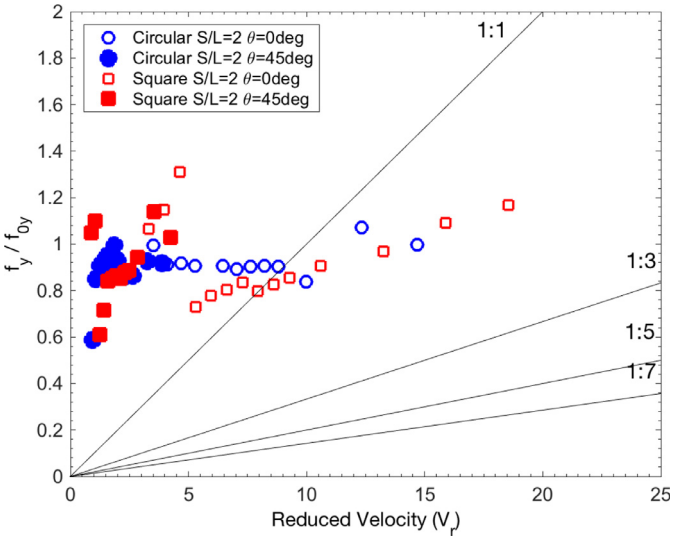

Fig. 23. Nondimensional frequency for the motions in the transverse direction for the array of cylinders with S/L = 2 with the reduced velocity adjustment to the single body projected face.

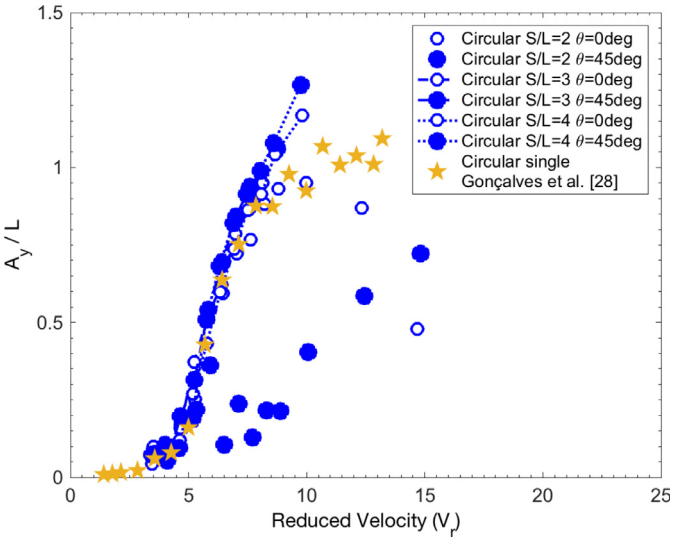

Fig. 24. Comparison of the nondimensional amplitudes of the motions in the transverse direction for the single cylinder and the 4-circular-column arrays.

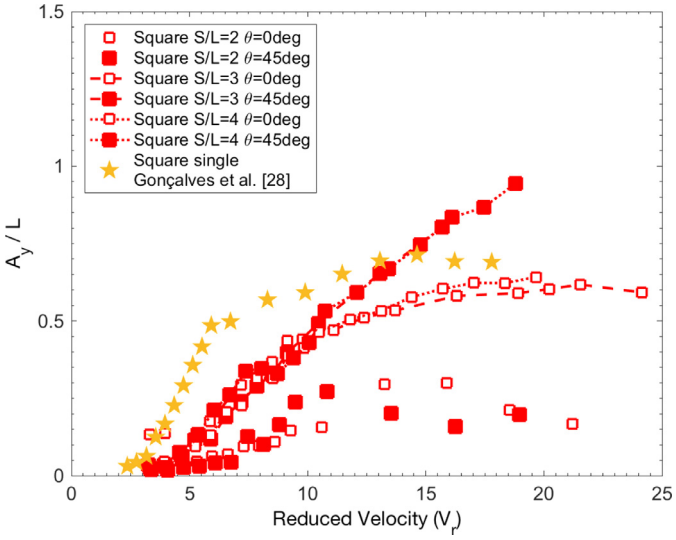

Fig. 25. Comparison of the nondimensional amplitudes of the motions in the transverse direction for the single cylinder and the 4-square-column arrays.

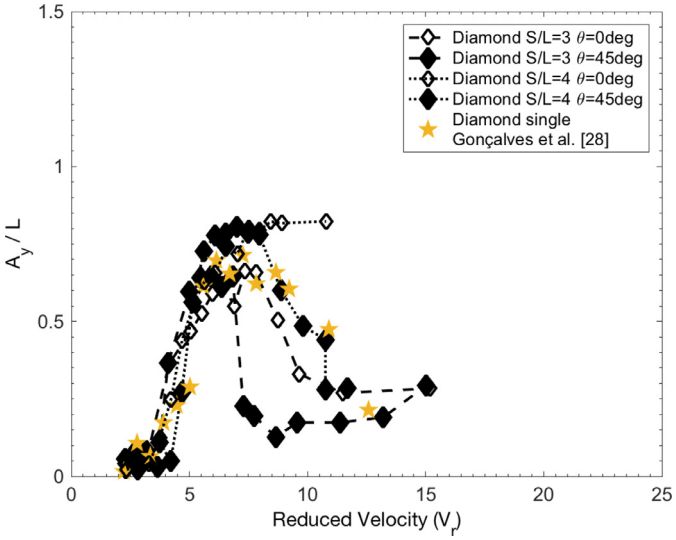

Fig. 26. Comparison of the nondimensional amplitudes of the motions in the transverse direction for the single cylinder and the 4-diamond-column arrays.

make some conclusions.

The amplitudes in the transverse direction, Fig. 18, showed different behaviors for the circular case with 0-deg when compared with the square ones. The amplitudes for the circular case with 0-deg presented a maximum around $V_r = 10$ and a decrease of amplitudes for higher reduced velocities; this behavior was similar to the resonance range in the VIM phenomenon.

In turn, it was not possible to determine a peak and resonance behavior for the square column cases; the behavior is not similar to the galloping phenomenon for all the range of reduced velocities tested due to a decrease in amplitudes for $V_r > 15$. In Fig. 18, the maximum values of the amplitudes in the transverse direction for $S/L = 2$ were A_y/L=0.95 and 0.30 for the circular and square cases with 0-deg incidence, respectively. As commented before, the 45-deg cases can be seen as a unique body with larger characteristic diameter; the correction of the reduced velocity and nondimensional amplitudes helped to consolidate the amplitude results, and it made the results similar to the 0-deg incidence ones for a small range of reduced velocities.

The amplitudes in the in-line direction, Fig. 19, showed a significant difference caused by the incidence angle. For circular cases with 0-deg incidence, it was possible to observe a resonance phenomenon of the in-line motion and, consequently, the presence of the amplitude drop and maximum amplitude $A_x/L = 0.3$. The value $V_r = 10$ is not a typical value of reduced velocity for the peak of the synchronization for the motions in the in-line direction. The interaction between the wakes and also the 3D structures due to the free end of low aspect ratio structures included multi-frequency structures on the flow, and the FIM could be considered far from the typical VIM or galloping phenomenon for this small spacing ratio, $S/L = 2$. For the square cases, the behavior of the amplitudes in the in-line the amplitudes kept growing for $V_r > 10$, which may confirm the galloping behavior for the square cases. The maximum amplitudes for the square cases were lower than for the circular ones, $A_x/L = 0.2$.

Considering a single body for 45-deg incidence and using the same procedure applied for the motions in the transverse to the motions in the in-line direction, the nondimensional amplitudes would be similar to 0-deg incidence ones for the new range of reduced velocities, see Fig. 20. Limitations in this conclusion were due to the small range of reduced velocity after applying the face dimension correction.

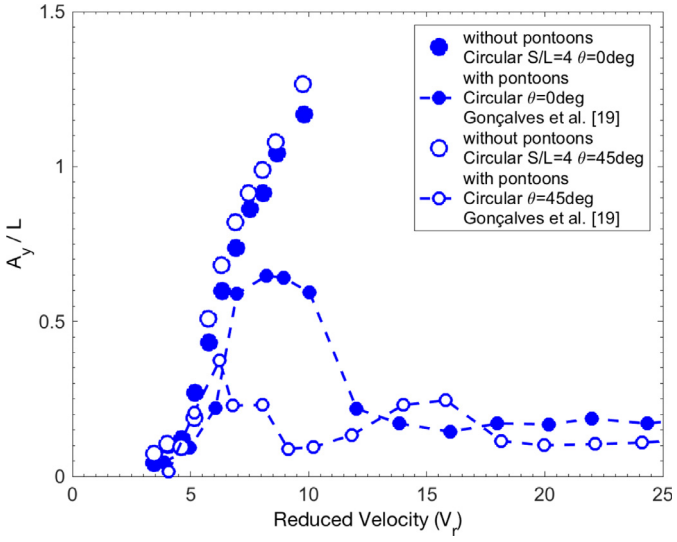

Fig. 27. Comparison of the nondimensional amplitudes of the motions in the transverse direction for the 4-circular-cylinders array and a deep-draft semi-submersible with pontoons and S/L = 4.

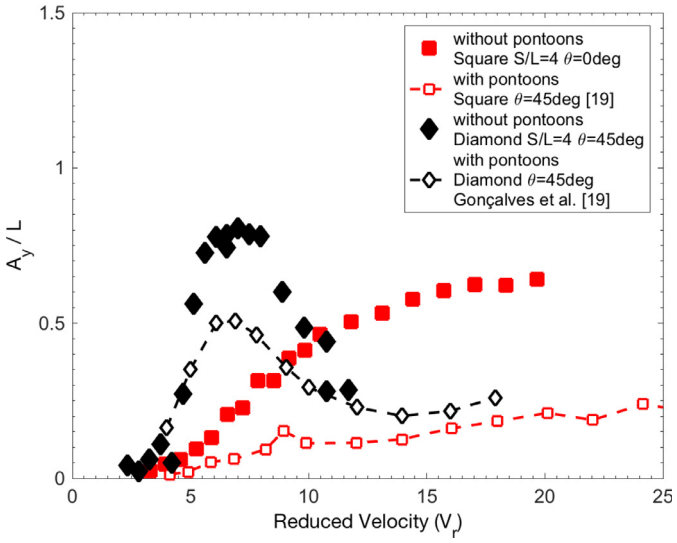

Fig. 28. Comparison of the nondimensional amplitudes for the motions in the transverse direction for the single cylinder case and the 4-cylinder array with square and diamond cylinders and a deep-draft semi-submersible with pontoons and S/L = 4.

The results of the amplitudes of the yaw motion for $S/L = 2$ are presented in Fig. 21. The maximum values of the amplitudes of the yaw motion were A_{yaw}= 4.2 and 2.2° for the circular and square cases, respectively. Similar behavior was observed for the 0 and 45-deg incidences. It was not possible to determine the nature of the FIM for this degree of freedom; more studies on lift and drag forces should be carried out to determine the VIM or galloping behavior.

Fig. 22 presents the nondimensional frequency for the array of 4-cylinders with $S/L = 2$, $\theta = 0$ and 45°, and different column geometries. Fig. 23 presents the correction of the nondimensional frequency using the new value of the face dimension, considering a single body for the 45-deg incidence.

For the square cylinder and 0-deg incidence, it was possible to see a similar galloping behavior close to the 1:3 synchronization regime. In the case of the 45-deg incidence, the range of reduced velocity was minimal, and no conclusion could be drawn. For the circular cylinder and 0-deg incidence, frequency results following the 1:1 synchronization regime were expected due to the similar VIM behavior presented for the motions in the transverse direction; therefore, the values were almost constant in the range $V_r < 10$. Because of this behavior, it was not possible to confirm the VIM phenomenon for the circular case and $S/L = 2$. As commented before, the multi-frequency flow around this condition altered the phenomenology of the FIM and needs to be better studied.

In Figs. 24–26, the results of the amplitudes in the transverse direction were consolidated to clarify the distance between column center effects, S/L= 2, 3 and 4 for the circular, square and diamond cases, respectively. The results were presented for all the column geometry cases for 0 and 45-deg incidences. The single column results were obtained from Gonçalves et al. [28].

The amplitudes in the transverse direction were practically the same for all the values of the distance between columns for the circular case with $S/L > 2$, see Fig. 24. Thus, the distance between columns did not affect this column geometry for the large distance between columns $S/L > 2$. On the other hand, the amplitude results were very different when comparing the cases of $S/L = 2$. This behavior occurred because the interference between the vortex shedding and wake was significant due to the proximity of the columns and also because the flow acted in the system as a unique body for the 45-deg incidence. The same behavior was observed for square column cases, see Fig. 25. Fujiwara et al. [29] verified similar conclusions when investigating a SS with four-circular columns with different column spacing ratio.

For the circular and diamond cases, see Figs. 24 and 26, the four-column array presented amplitudes in the transverse direction higher than the single circular cylinder. The VIM-dominated response observed for circular and diamond columns, as more broadly discussed before, promoted a favorable vortex-shedding interaction in the presence of four columns for $S/L > 2$ and the resonance region was larger. For the square case, see Fig. 25, the single column presented the highest amplitudes in the transverse direction. The galloping-dominated response was observed for square columns and the lift forces modified in the presence of four columns such that the amplitudes in the transverse direction decreased when compared to a single column.

Figs. 27 and 28 present the comparison of the nondimensional amplitudes in the transverse direction of the 4-column array and a DD – deep-draft semi-submersible case with four pontoons. The results of the VIM of the deep-draft semi-submersible were extracted from Gonçalves et al. [12]. The distance between columns was the same for all the cases compared, i.e., $S/L = 4$. The comparison of results showed that the amplitudes were lower for the cases with the presence of pontoons. The effect of the presence of the pontoon was very marked, but the nature of the FIM-dominated response (VIM or galloping) was not affected. It is important to evaluate the damping level due to the pontoon presence since the increase in the damping level caused a decrease in the amplitudes. This result is significant for designing offshore platforms since the presence of pontoon is frequent, and it can thus benefit the FIM for these kinds of platforms. The presence of the pontoons must be better investigated because the FIM response is sometimes larger than the cases without pontoons, as presented by Gonçalves et al. [30].

4. Conclusions

Experimental studies were conducted in a towing tank to evaluate the FIM behavior of the four-column arrays. Three different parameters were experimented to understand their effects on the FIM, such as column geometry (circular, square and diamond), the distance between column centers (S/L= 2, 3 and 4) and current incidence angles (θ = 0 and 45°).

The column geometry significantly affected the FIM behavior of the four-column arrays. The most considerable amplitudes were observed for the circular case for the motions in the transverse direction, in-line direction, and yaw. For the transverse direction, VIM-dominated response was confirmed for the circular and diamond cases; however, the

galloping behavior was confirmed for the square case. For the yaw motions, conclusions are still open and must be better investigated.

The distance between column centers showed a different behavior for $S/L = 2$, in which the columns acted as a single body to the flow incidence for the 45-deg incidence, and significantly affected the wake inference for 0-deg incidence. For S/L= 3 and 4, the results were practically the same, which allows concluding that for $S/L > 2$, the effect of the distance between column centers can be neglected.

For $S/L > 2$, it was possible to conclude that the nature of the FIM, VIM or galloping-dominated response, is due to the column section geometry and not related to the current incidence angles. The current incidence angle was responsible for affecting the amplitudes for high values of reduced velocity, $V_r > 10$.

The comparison of the results of the amplitudes in the transverse direction presented herein with previous works in the literature on VIM of a single cylinder showed that the highest amplitudes in the transverse direction occurred for the four-column arrays for the circular and diamond cases, i.e., in the cases in which VIM-dominated response occurred. Moreover, the highest amplitude happened for the single column for the square case, i.e., in the case in which galloping-dominated response occurred.

The comparison of the present results with the VIM of a DD SS with pontoons highlighted the significant effect of the presence of the pontoon, which accounted for changing the flow around the system and, consequently, the FIM behavior of the system. The presence of pontoons was responsible for a substantial decrease of the amplitudes in the transverse direction, mainly for $V_r > 5$.

All these conclusions showed the importance of better understanding the FIM-dominated response of the array of columns and how the parameters can influence the motion amplitudes. Better knowledge about the nature of the FIM can help to find solutions to mitigate the FIM. The results presented here are essential for designing floating offshore platforms and FOWT and can also provide benchmark data for CFD.

Declaration of Competing Interest

There is no conflict of interest in this work.

Acknowledgments

The first author acknowledges the CNPq – the Brazilian National Council for Research for grant 200096/2017–6 and the JSPS - Japan Society Promotion of Science KAKENHI Grant Number JP18F18355 for supporting this work. The first author thanks the JSPS for the grant as JSPS International Research Fellow (P18355, Graduate School of Engineering, The University of Tokyo).

The authors would like to thank JASNAOE – The Japan Society of Naval Architects and Ocean Engineers for the opportunity and support given throughout the project “Brazil-Japan Collaborative Research Program 2016/2017″ supporting the internship period of the authors Lopes, PPSP, Hannes, NH, and Chame, MEF during the experiment period in Japan.

The authors would also like to thank the student Marques, MA from the UFPE – Federal University of Pernambuco for helping with the post-processing data and Cenci, F from UFSC – Federal University of Santa Catarina for his help during the image developments.

Supplementary materials

Supplementary material associated with this article can be found, in the online version, at doi:10.1016/j.apor.2019.102019.

References

[1] R.D Blevins, Flow-Induced Vibration, Second ed., Krieger Publishing Company, 2001, pp. 104–152.
[2] J. Zhao, J.S. Leontini, D.L. Jacono, J Sheridan, Fluid–structure interaction of a square cylinder at different angles of attack, J. Fluid Mech. 747 (2014) 688–721.
[3] A.L.C. Fujarra, G.F. Rosetti, J. Wilde, R.T Gonçalves, State-of-art on vortex-induced motion: a comprehensive survey after more than one decade of experimental investigation, Proceedings of the ASME 2012 31st International Conference on Ocean, Offshore and Arctic Engineering, OMAE2012-83561. Rio de Janeiro, RJ, Brazil, 2012.
[4] R.R. Dijk, A. Magee, S. Perryman, J Gebara, Model test experience on vortex induced vibrations of truss spars, Proceedings of the Offshore Technology Conference, OTC2003-15242, Houston, USA, 2003.
[5] M. Irani, L. Finn, Improved strake design for vortex induced motions of spar platforms, Proceedings of the ASME 2005 24th International Conference on Offshore Mechanics and Arctic Engineering, OMAE2005-67384, Halkidiki, Greece, 2005.
[6] D. Roddier, T. Finnigan, S Liapis, Influence of the reynolds number on spar vortex induced motions (VIM): multiple scale model test comparisons, Proceedings of the 28th International Conference on Ocean, Offshore and Arctic Engineering, OMAE2009-79991, Honolulu, HI, USA, 2009.
[7] L.V.S. Sagrilo, M.Q. Siqueira, T.A.G. Lacerda, G.B. Ellwanger, E.C.P. Lima, E.F.N Siqueira, VIM and wave-frequency fatigue damage analysis for SCRs connected to monocolumn platforms, Proceedings of the 28th International Conference on Ocean, Offshore and Arctic Engineering, OMAE2009-79431, Honolulu, HI, USA, 2009.
[8] R.T. Gonçalves, A.L.C. Fujarra, G.F. Rosetti, K Nishimoto, Mitigation of vortex-induced motion (VIM) on a monocolumn platform: forces and movements, J. Offshore Mech. Arct. Eng. 132 (4) (2010) 041102.
[9] M. Saito, T. Fujiwara, K Maeda, An experimental investigation of cylindrical floater vim in current and waves, Proceedings of the 33rd International Conference on Ocean, Offshore and Arctic Engineering, OMAE2014-23702. San Francisco, CA, USA, 2014.
[10] M.A.A. Rahman, K. Thiagarajan, Vortex-induced vibration of cylindrical structure with different aspect ratio, Proceedings of the 17th International Offshore and Polar Engineering Conference, ISOPE. Anchorage, Alaska, USA, 2013.
[11] M. Zhao, L. Cheng, Vortex-induced vibration of a circular cylinder of finite length, Phys. Fluid 26 (2014) 015111–1-26.
[12] R.T. Gonçalves, J.R. Meneghini, A.L.C Fujarra, Vortex-induced vibration of floating circular cylinders with very low aspect ratio, Ocean Eng. 154 (2018) 234–251.
[13] R.T. Gonçalves, D.M. Gambarine, F.P. Figueiredo, F.V. Amorim, A.L.C Fujarra, Experimental study on flow-induced vibration of floating squared section cylinders with low aspect ratio, part I: effects of incidence angle, Proceedings of the ASME 34th International Conference on Ocean, Offshore and Arctic Engineering, OMAE2015-41008, St. Johns, NL, Canada, 2015.
[14] R.T. Gonçalves, D.M. Gambarine, A.M. Momenti, F.P. Figueiredo, A.L.C Fujarra, Experimental study on flow-induced vibration of floating squared section cylinders with low aspect ratio, part II: effects of rounded edges, Proceedings of the ASME 2016 35th International Conference on Ocean, Offshore and Arctic Engineering, OMAE2016-54813, Busan, South Korea, 2016.
[15] M. Irani, T. Jennings, J. Geyer, E Krueger, Some aspects of vortex induced motions of a multi-column floater, Proceedings of the ASME 34th International Conference on Ocean, Offshore and Arctic Engineering, OMAE2015-41164, St. John's, NL, Canada, 2015.
[16] O.J. Waals, A.C. Phadke, S Bultema, Flow induced motions of multi column floaters,”, Proceedings of the ASME 26th International Conference on Offshore Mechanics and Arctic Engineering, OMAE2007-29539. San Diego, California, USA, 2007.
[17] R.T. Gonçalves, G.F. Rosetti, A.L.C. Fujarra, A.C Oliveira, Experimental study on vortex-induced motions of a semi-submersible platform with four columns, Part I: Effects of Current Incidence Angle and Hull Appendages 54 Ocean Engineering, 2012, pp. 150–169.
[18] F. Lamas, M.A.M. Ramirez, A.C Fernandes, Yaw galloping of a TLWP platform under high speed currents by analytical methods and its comparison with experimental results, Proceedings of the ASME 2017 36th International Conference on Offshore Mechanics and Arctic Engineering, OMAE2017-61909, Trondheim, Norway, 2017.
[19] R.T. Gonçalves, A.L.C. Fujarra, G.F. Rosetti, A.M. Kogishi, A Koop, Experimental study of the column shape and the roughness effects on the vortex-induced motions of deep-draft semi-submersible platforms, Ocean Eng. 149 (2018) 127–141.
[20] M. Liu, L. Xiao, H. Lu, J Shi, Experimental investigation into the influences of pontoon and column configuration on vortex-induced motions of deep-draft semi-submersibles, Ocean Eng. 123 (2016) 262–277.
[21] M.A.M. Ramirez, A.C. Fernandes, Novel experimental investigation on vortex induced motions of a tension leg platform, Proceedings of the ASME 35th International Conference on Ocean, Offshore and Arctic Engineering, OMAE2016-54530, Busan, South Korea, 2016.
[22] M. Liu, L. Xiao, Y. Kou, F Wu, Experimental and numerical studies on the excitation loads and vortex structures of four circular section cylinders in a square configuration, Ships Offshore Struct. 11 (7) (2016) 734–746.
[23] R.T. Gonçalves, S. Hirabayashi, H Suzuki, Experimental study on flow around an array of four circular cylinders, Proceedings of IEEE Techno-Ocean, Kobe, Japan, 2016.
[24] R.T. Gonçalves, S. Hirabayashi, H Suzuki, Experimental study on flow around an array of four cylinders with different section geometries, Proceedings of the ASME 2017 36th International Conference on Ocean, Offshore and Arctic Engineering, OMAE2017-61014, Trondheim, Norway, 2017.
[25] R.T. Gonçalves, M.E. Chame, N.H. Hannes, P.P.S.P. Lopes, S. Hirabayashi, H. Suzuki, FIM – Flow-induced motions of three-column platforms, Int. J. Offshore Polar Eng. (2020) in press.

[26] C.P. Pesce, G.A. Amaral, G.R Franzini, Mooring system stiffness: a general analytical formulation with an application to floating offshore wind turbines. Proceedings of the ASME 1st International Offshore Wind Technical Conference,IOWTC2018-1040, San Francisco, CA, 2018.

[27] Williamson, C.H.K., Govardhan, R. Vortex-induced vibrations. Annu. Rev. Fluid Mech.2004;36, pp. 413–455.

[28] R.T. Gonçalves, M.E.F. Chame, N.H. Hannes, P.P.S.P. Lopes, H. Suzuki, S Hirabayashi, Experimental flow-induced motions of array of floating cylinders with circular, square and diamond sections. Proceedings of the 24th ABCM International Congress of Mechanical Engineering, COBEM-2017-0441, Curitiba, PR, Brazil, 2017.

[29] T. Fujiwara, T. Nimura, K. Shimozato, R Matsui, VIM model test and assessment on a semi-submersible type floater with different column intervals. Proceedings of the ASME 35th International Conference on Ocean, Offshore and Arctic Engineering, OMAE2016-54308. Busan, South Korea, 2016.

[30] R.T. Gonçalves, H. Suzuki, F. Cenci, A.L.C. Fujarra, S Hirabayashi, Experimental study of the effect of the pontoon presence on the flow-induced motion of a semi-submersible platform with four square columns. Proceedings of the ASME 38th International Conference on Ocean, Offshore and Arctic Engineering, OMAE2019-95250. Glasgow, Scotland, UK, 2019.